A carbon material doped with both porous FeO_x and N as an efficient catalyst for oxygen reduction reactions

GAO Jian[1,2], WANG Xin-yao[1], MENG Ling-xin[1], YIN Zhen[3], MA Na[3,*], TAN Xiao-yao[1], ZHANG Peng[2,4,*]

（1. *State Key Laboratory of Separation Membranes and Membrane Processes*, *Tianjin Key Laboratory of Green Chemical Engineering Process Engineering*, *Department of Chemical Engineering*, *Tiangong University*, *Tianjin* 300387, *China*;
2. *Haian Nanjing University High Tech Institute*, *Haian* 226600, *China*;
3. *College of Chemical Engineering and Materials Science*, *Tianjin University of Science and Technology*, *Tianjin* 300457, *China*;
4. *School of Environmental Science and Engineering*, *Tiangong University*, *Tianjin* 300387, *China*）

Abstract: To replace precious metal oxygen reduction reaction (ORR) electrocatalysts, many transition metals and N-doped carbon composites have been proposed in the last decade resulting in their rapid development as promising non-precious metal catalysts. We used Ketjenblack carbon as the precursor and mixed it with a polymeric ionic liquid (PIL) of $[Hvim]NO_3$ and $Fe(NO_3)_3$, which was thermally calcined at 900 °C to produce a porous FeO_x, N co-doped carbon material denoted FeO_x-N/C. Because the PIL of $[Hvim]NO_3$ strongly combines with and disperses Fe^{3+} ions, and NO^{3-} is thermally pyrolyzed to form the porous structure, the FeO_x-N/C catalyst has a high electrocatalytic activity for the ORR in both 0.1 mol L^{-1} KOH and 0.5 mol L^{-1} H_2SO_4 electrolytes. It was used as the catalyst to assemble a zinc-air battery, which had a peak power density of 185 mW·cm^{-2}. Its superior electrocatalytic activity, wide pH range, and easy preparation make FeO_x-N/C a promising electrocatalyst for fuel cells and metal-air batteries.

Key words: Oxygen reduction reaction; Ionic liquid; Porous carbon; Electrocatalysis; FeO_x; N co-doping

1 Introduction

Because of the high theoretical energy density, the fuel cell and metal-air battery (MAB) are considered as promising new power sources to cope with the global energy crisis[1]. In the fuel cell and MAB, the oxygen reduction reaction (ORR) is a crucial electrochemical reaction. However, the ORR is sluggish in kinetics and needs electrocatalysts[2]. Despite the high catalytic efficiency, Pt-based catalysts have largely prohibited the large-scale applications due to their high price and poor durability[3]. Therefore, a lot of work has been conducted to develop the non-precious metal catalysts (NPMCs) to replace the existing Pt-based catalysts.

Among alternative NPMCs, the transition metal loaded on nitrogen-doped carbon (TM-N/C) materials attract intensive interest and hold the great promise to work in the place of the Pt-based electrocatalysts[4–6]. As an ideal carbon precursor, Ketjenblack carbon (KB) features good electronic conductivities, large specific surface area, and good commercial availability, which is widely investigated as the ORR catalyst by modifying with metal and/or heteroatoms[4,7]. For instance, urea was used as N source to prepare the N-doped KB, which was further used to fabricate a Fe, Ag-N-KB electrocatalyst for ORR[8]. The Cu-N-KB[9] and the Fe(or Co)-N-KB[10] were separately obtained by introducing N, N-dimethylformamide and ethylene diamine tetraacetic acid into the structure of KB, both of which were determined to efficiently catalyze the ORR.

In recent years, polymeric ionic liquids (PILs) are rapidly developed as good precursors for NPMCs[11,12]. On the one hand, heteroatoms in PILs can spontaneously serve as the heteroatom resources. On the other hand, the negligible volatility enables the high doping efficiency. Therefore, various PILs are

Received date: 2024-04-10; **Revised date:** 2024-07-05
Corresponding author: MA Na, Ph.D. E-mail: mana@tust.edu.cn;
ZHANG Peng, Associate Professor. E-mail: pengzhang@tiangong.edu.cn
Author introduction: GAO Jian, Professor. E-mail: gaojian@tiangong.edu.cn

widely investigated to synthesize the heteroatom-doped carbon materials with high ORR activity[13–15]. These unique properties inspire us to utilize the PIL to modify KB to prepare the TM-N/C catalyst for ORR.

In this work, both the PIL of $[Hvim]NO_3$ and $Fe(NO_3)_3$ are used to modify the KB to yield a mixture, which is then thermally calcined to prepare a Fe, N co-doped carbon material (FeO_x-N/C). As shown in Fig. 1, the PIL of $[Hvim]NO_3$ can trap and combine Fe^{3+} to efficiently disperse the Fe species in the carbon product. Meanwhile, the NO_3^- will decompose at high temperature to generate abundant pores. Consequently, the resultant Fe, N co-doped carbon exhibits the promising electrocatalytic activity for ORR.

2 Experimental

2.1 Preparation of the catalyst

The IL was prepared as follows: 0.1 mol vinylimidazole was added dropwise into 0.1 mol HNO_3 (65%, mass fraction) under magnetic stirring in a one-necked flask immersed in a water bath below 10 °C. The system was agitated for an additional hour after the vinylimidazole addition. The water bath was then heated to 50 °C and stirred for 4 h to achieve a viscous liquid. The liquid was characterized with 1H NMR (Fig. S1 in the supporting information) to confirm the structure. Then 0.02 mol $Fe(NO_3)_3$ and 2 g KB were added to the ionic liquid (dissolved in water of 10 mL) and stirred for 2 h. The mixture was then dried at 60 °C for 24 h and transferred to a tube furnace for pyrolysis at 900 °C for 1 h in a N_2 flow rate of 60 mL·min^{-1}. After cooling to room temperature, a black product was collected, grounded and denoted as FeO_x-N/C. For comparison, a sample named NC was prepared without adding $Fe(NO_3)_3$ under similar conditions.

2.2 Catalyst characterization

The morphology of the FeO_x-N/C was observed with scanning electron microscopy (SEM, Hitachi S4800, JEM-F200) and transmission electron microscopy (TEM, Hitachi H7650). Elemental distribution of the FeO_x-N/C was obtained by a high-angle annular dark-field scanning transmission electron microscope (HAADF-STEM, JEOL JEM-2100F). A Brunauer-Emmett-Teller (BET, Quantachrome Autosorb-iQ) analyzer was used to acquire nitrogen adsorption-desorption isotherms at −196 °C. X-ray diffractometer (XRD, Bruker D8 ADVANCE) was used to study the crystal structure and phase composition. The surface structure was measured by X-ray photoelectron spectroscopy (XPS, ThermoFisher K-Aepna). Raman spectroscopy (Raman, HORIBA XploRA PLUS) was used to analyze the carbon structure of the FeO_x-N/C.

2.3 Electrochemical measurement

Electrochemical tests were performed with a rotating disk electrode (RDE) and a rotating ring and disc electrode (RRDE, Pine Research) in a standard three-electrode system connected to a working station (CHI 760E, Chenhua, Shanghai) at 25 °C with KOH aqueous solution (0.1 mol L^{-1}). The working elec-

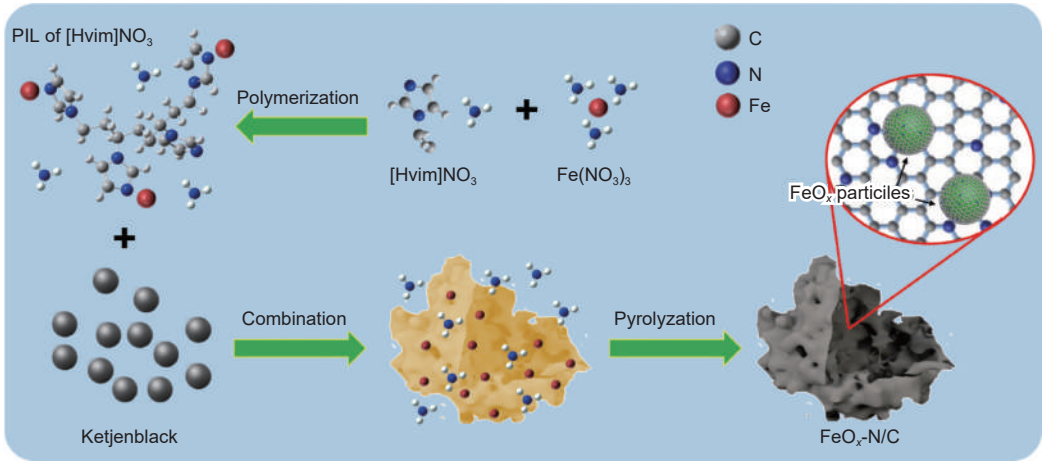

Fig. 1　Synthesized illustration of the FeO_x-N/C catalyst

trode (WE) was prepared as previously described[16]. Briefly: the prepared catalyst (working electrode 1.25 mg), Nafion (5%, 25 μL) and ethanol (225 μL) were mixed and ultrasonicated for 30 min to achieve a homogeneous black catalyst ink. 10 μL of this ink was then dropped onto a glassy carbon electrode to obtain a working electrode with a loading of 0.25 mg·cm^{-2}. A Hg/HgO electrode and a Pt electrode were employed as the reference electrode and counter electrode, respectively. All electrochemical tests were performed in an oxygen or nitrogen-saturated electrolyte, and the measured potentials were converted to those against the reversible hydrogen electrode (RHE): $E_{RHE} = E_{Hg/HgO} + 0.93$. The FeO_x-N/C was also tested in the electrolyte of 0.5 mol L^{-1} H_2SO_4 with the Ag/AgCl reference electrode, and the potential was converted to V by $E_{RHE} = 0.1976 + 0.059\ pH + E_{Ag/AgCl}$[17]. The commercial Pt/C catalyst (20%) was tested as bench mark.

To check the applicability of the catalyst, a Zn-Air battery (ZAB, effective area: 1 cm^2) was assembled with the FeO_x-N/C as the ORR catalyst. The assembly method was described previously[18]. Firstly, 5 mg catalyst, 350 μL of ethanol, and 50 μL Nafion solution (5%) were mixed and sonicated for 45 min to prepare a catalyst ink, 80 μL of which was then coated onto a carbon sheet to obtain a cathode (catalyst loading: 1 mg·cm^{-2}). A Zn sheet was used as the anode, while a mixture solution of 6 mol L^{-1} KOH and 0.2 mol L^{-1} $Zn(CH_3COO)_2$ was applied as the electrolyte. After stabilized for 60 min, the assembled battery was measured for discharging behavior with a Gamry electrochemistry station. The stability of ZAB was tested for 2 h at 80 mA. Cycling performance was tested on a battery testing system using Land-CT3002A.

3 Results and discussion

In the imidazolium PILs, the cation can form N-doped carbon (N/C), and Fe^{3+} become FeO_x. In addition, the NO_3^- in the system decomposed at around 180 °C to generate pores. Therefore, a Fe, N co-doped carbon material, i.e. FeO_x-N/C, was finally prepared after pyrolysis.

Fig. 2a shows a representative SEM image of the FeO_x-N/C. A particle with irregular surface can be observed. Fig. 2b shows an enlarged image of the area in Fig. 2a in the red-colored circle. Pores and cross-linked channels, some of which displayed in green circles can be observed. This structure would favor the catalytic performance.

In the TEM image of the FeO_x-N/C (Fig. 2d), many particles can be found to be dispersedly supported on the carbon. The HRTEM image the particle (Fig. 2e) clearly represents a typical core/shell structure, of which the lattice spacings of the particle and the shell are measured as 0.15 and 0.36 nm, which are assigned to Fe_3O_4 (440)[19] and graphite (002)[20] , respectively. Compared with normal particles, this carbon shell not only greatly enhances the electron-transferred efficiency due to the strong interaction with the FeO_x particle, but also protects the FeO_x core from erosion[21]. Therefore, this carbon-parceled Fe particles could be expected to improve both the electrochemical stability and the catalytic activity of this FeO_x-N/C. In the HAADF-STEM image and corresponding elemental mappings (Fig. 2f-i), the supported FeO_x particles can be clearly identified. Besides, the homogeneous dispersion of C and N indicates the uniformly doping of N to the carbon.

Fig. 3a shows a type IV N_2 adsorption-desorption isotherm for the Fe-N/C, indicating the abundant micropore and mesopore structure[22]. The pore size distribution (inset of Fig. 3a) proves that the pore size of the Fe-N/C generally varies in the range of 1.5–8.0 nm. The micro pores (<2 nm) are important to host the N-Fe active sites[23], while the mesoporous structure facilitates reactants to reach the active sites with minor diffusion limitation[24]. Therefore, the well-defined mesopores and micropores can make more active sites accessible and favor the mass and charge transport[25]. From the N_2 adsorption isotherm, the BET surface area of the Fe-N/C is confirmed as 678.7 m^2·g^{-1}, being comparable to some reported ORR catalysts, such as the MOF-derived Fe-N/C with 400 m^2·g^{-1}[26], ZIF-8 derived Fe-N/C with 600–800 m^2·g^{-1}[27].

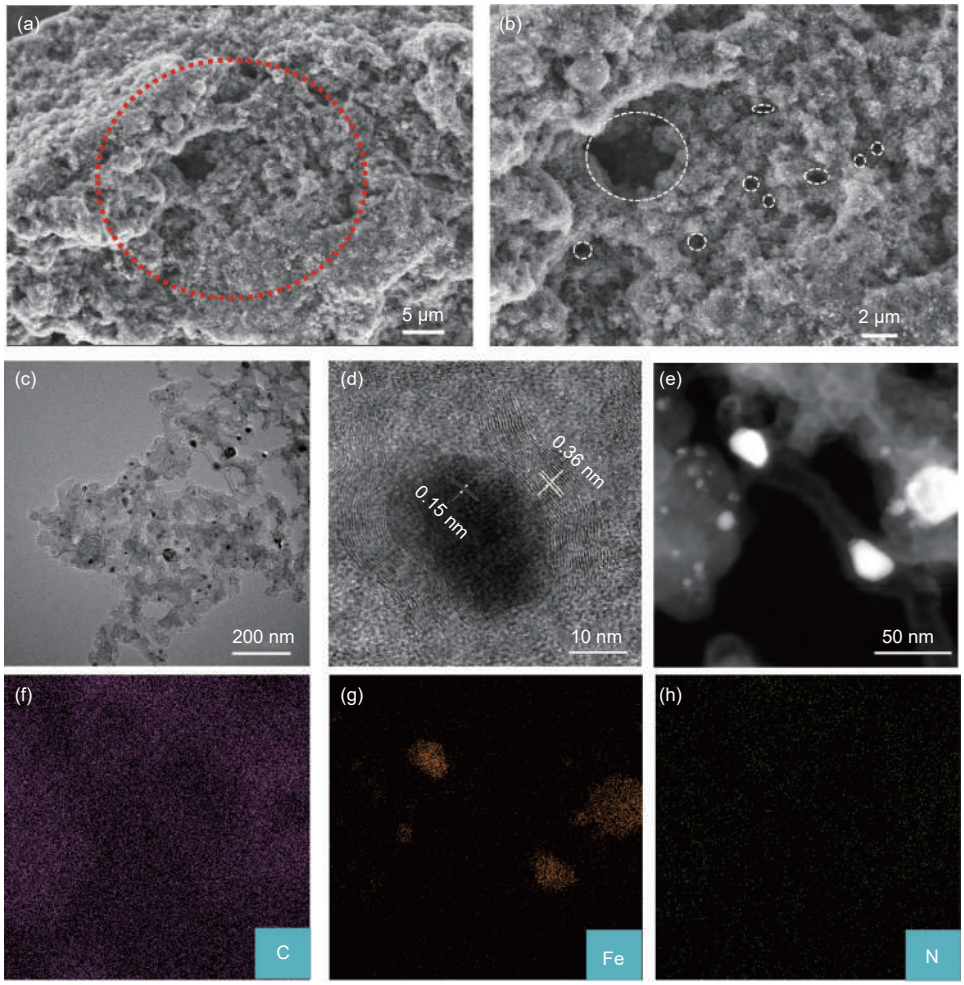

Fig. 2　(a, b) SEM images, (c) TEM, (d) HRTEM images, (e) images of HAADF-STEM for the FeO_x-N/C. (f-h) Elemental mapping of C, Fe and N in the FeO_x-N/C

The electrochemically active surface area (ECSA) is estimated using the double-layer capacitance (C_{dl}) derived from various CV curves at scan rates of 1–500 $mV \cdot s^{-1}$ (inset of Fig 3b)[28]. A nearly linear relationship (Fig. 3b) can be obtained by plotting the average current density (A_J) ($A_J = (J_{anodic} - J_{cathodic})/2$) at 0.6 V *vs.* the scan rate, the slope of which represents the specific capacitance (C_{dls}) value (17.8 $mF \cdot cm^{-2}$)[29]. The surface area and catalyst loading of the working electrode are 0.196 25 cm^2 and 0.05 mg, the ECSA could be calculated as 174.5 $m^2 \cdot g^{-1}$, where the specific capacitance (C_s) of real surface area is typically 0.4 $F \cdot m^{-2}$ in the alkaline electrolyte. This high ECSA of the FeO_x-N/C can be expected to significantly enhance its electrocatalytic activity.

In the XRD pattern of the FeO_x-N/C (Fig. 3c), the diffraction peak at ~25° is the (002) face of graphite[30]. Besides, other strong peaks at 35.7°, 37.8°, 39.8°, 40.5°, 42.8°, 43.8°, 44.6°, 45.8°, 49.8°, and 51.8° suggest that the supported FeO_x particles have a mix crystal composition of Fe_3O_4[19] and Fe_2O_3[31]. The Raman spectrum of the FeO_x-N/C (Fig. 3d) includes two peaks at 1 346 and 1 589 cm^{-1}, corresponding to the bands of *D* and *G*, respectively. *D* band is attributed to the disordered structure, indicating that heteroatoms are successfully doped, and the *G* band comes from the vibration of all sp^2 hybrid C atoms. Raman result proves that the FeO_x-N/C has a defective carbon structure with the high electrocatalytic activity.

The survey XPS spectrum of the FeO_x-N/C is presented in Fig. 4a. No obvious Fe signal implies the low content of Fe (0.16%, atomic percent). As for C structure (Fig. 4b), besides the peaks at 290.2 eV

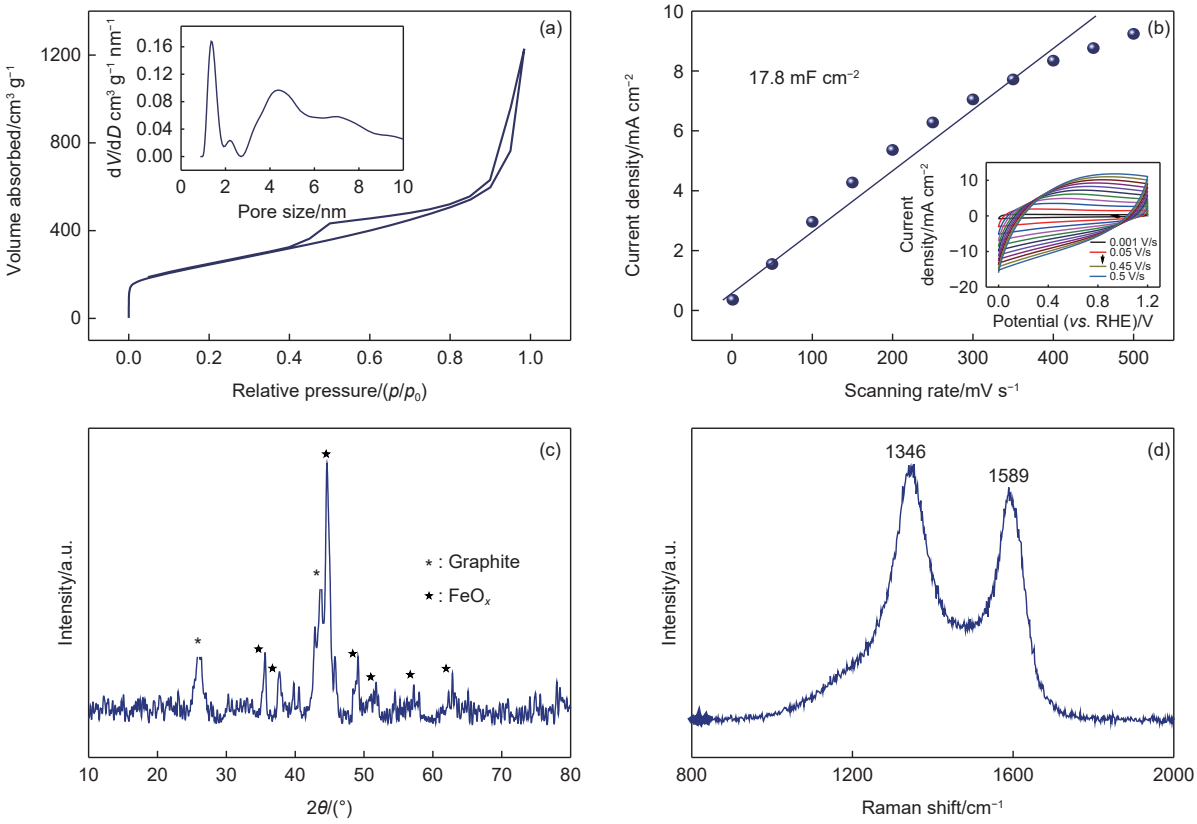

Fig. 3 (a) N_2 adsorption-desorption isotherm of the FeO_x-N/C, inset: the pore size distribution, (b) non-Faradic current density *vs.* scanning rate plot of the FeO_x-N/C, inset is its CV curves at various scan rates, (c) XRD pattern and (d) Raman spectrum of the FeO_x-N/C

(9.55%) from adsorbed C—O species[32], the peaks at 288.1 eV (4.18%), 286.5 eV(7.25%), 284.9 eV and 284.0 eV (57.07%) are related to the C—N[33], pyrrolic carbon[33], C—O_x species[34], and the graphitic carbon[35]. Therefore, the carbon structure of the FeO_x-N/C is mainly composed of graphitic carbon, meanwhile the N atoms are introduced into the carbon as various states. In the XPS spectrum for N 1s (Fig. 4c), the peak of N can be deconvoluted into several bands: the peaks at 406.9 and 404.1 (totally 16.9%) are attributed to the N—O_x[36,37]. The peak at 402.3 eV (10.3%) is related to pyridinic N bonded with O[38]. The peak at 401.1 eV (24.3%), 399.7 eV (18.5%) and 398.7 eV (5.49%) come from the graphitic N, pyrrolic N and pyridinic N, respectively. The graphitic-N helps the electron transport from the carbon bands of electronic to the O orbitals of antibonding, thus elevating the catalytic activity[39]. Both the pyrrolic N and pyridinic N are active for the ORR[16]. Besides, the peak at 397.3 eV (18.45%) should be assigned to N-Fe nitrides[40]. Therefore, the FeO_x-N/C catalyst is endowed with abundant ORR active sites, including Fe-N, graphitic N, pyrrolic N and pyridinic N.

The ORR activity of the FeO_x-N/C was first stud-

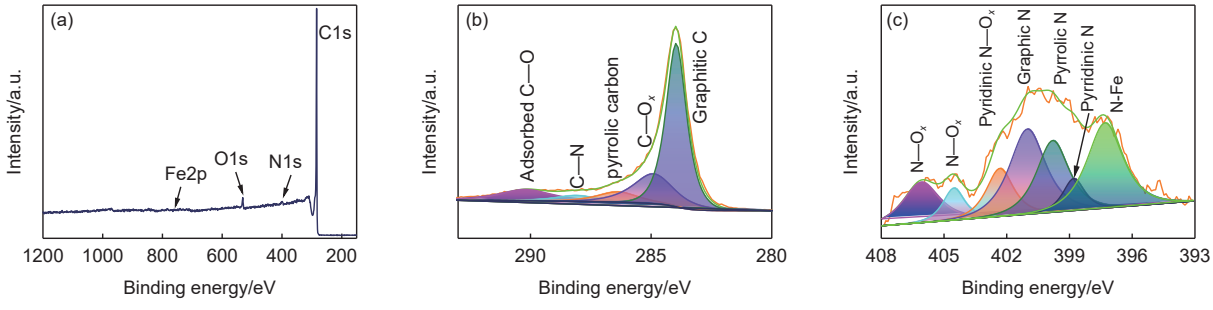

Fig. 4 XPS spectra of the FeO_x-N/C for (a) whole survey, (b) C 1 s and (c) N 1 s

ied in an electrolyte (0.1 mol L^{-1} KOH) saturated with N_2 and O_2, and the CV plots are recorded in Fig. 5a. A featureless semi square curve is displayed after the electrolyte was purged with N_2. Nevertheless, the reduction current increases obviously at 1.0 V after the electrolyte was purged with oxygen, indicating that the FeO_x-N/C is active for the ORR.

The LSV curve of the FeO_x-N/C at 1 600 r min^{-1} is shown in Fig. 5b, and commercial Pt/C catalyst is measured also for comparison. The onset potential of the FeO_x-N/C is 1.05 V and equal to that of the Pt/C. Meanwhile, the half-wave potential ($E_{1/2}$) of the FeO_x-N/C (0.87 V) is comparable to those reported electrocatalysts such as highly dispersed Fe-N_x (~0.83 V)[1], Pomegranate-like Co_3O_4 (0.84 V)[41], WC-Co@NC (0.87 V)[42] and single-atom Co-N_4 (0.8 V)[43].

Although the half-wave of the FeO_x-N/C is slightly lower than that of the commercial Pt/C of 0.88 V, the much lower cost of the FeO_x-N/C still offers it potential as alternative ORR catalyst. To investigate the role of the Fe in the catalyst, the NC was prepared and investigated as shown in Fig. 5b. The NC also shows profound catalytic performance as displayed. Therefore, the N—C and Fe—N work together to offer the obtained catalytic performance. However, the activity is much lower than that of FeO_x-N/C, implying the dominating role of the Fe species in the catalyst.

The LSVs at all rotational speeds (Fig. 5c) show that a platform diffusion-limited current is well-developed, thus the FeO_x-N/C performs well in the high potential range. Moreover, the LSVs are nearly aligned with one another, implying the first order kinetics for the ORR reaction toward the O_2 concentration. The number of transferred electrons (n) for the ORR is estimated to vary from 3.70 to 3.85 with the Koutecky-Levich (K-L) equation, which falls in the range of 3.2–3.9 for the 4-electron range[44]. It is concluded that the ORR on the FeO_x-N/C is a $4e^-$ pathway reaction, which is preferred for the application in fuel cells.

The n was further investigated with rotating ring-disk electrode (RRDE) technology, and the LSVs at 1 600 r min^{-1} are displayed in Fig. 5d. A high disk and low ring current density can be observed, and the disk current reaches −4.8 mA·cm^{-2}, while the ring current density is merely 0.04 mA·cm^{-2}, implying the low generation of H_2O_2. The HO_2^- % and n were calculated with the Equations (1) and (2).

$$HO_2^-\% = 200\frac{|I_d/N|}{|I_r/N| + |I_d|} \quad (1)$$

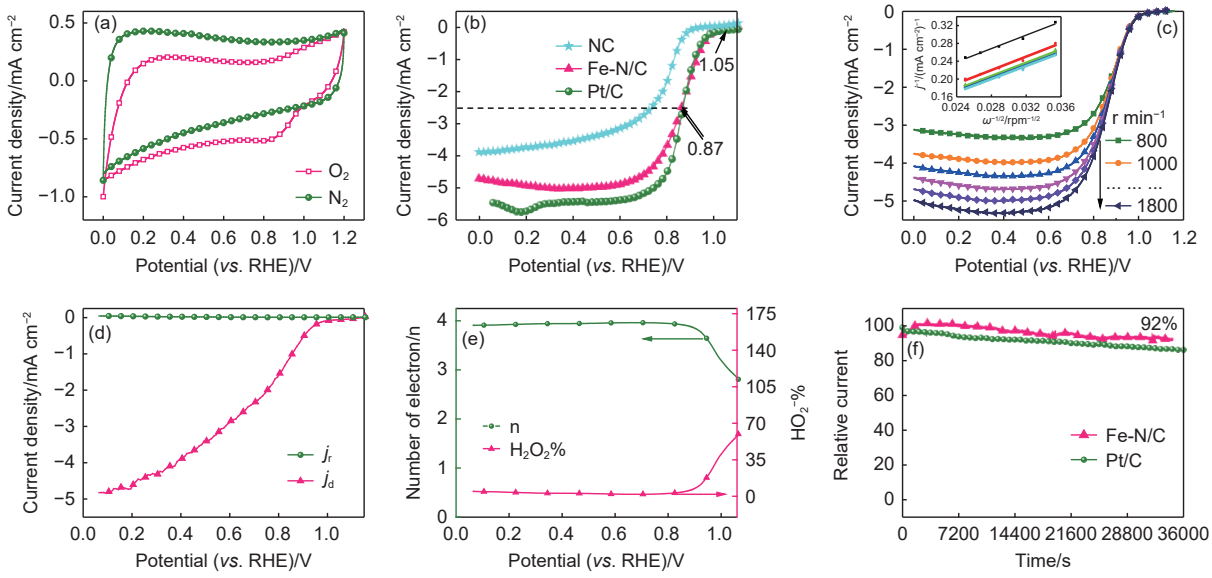

Fig. 5　(a) CV curves of the FeO_x-N/C in N_2 and O_2 saturated KOH electrolytes (0.1 mol L^{-1}). (b) LSV for the FeO_x-N/C, NC, and Pt/C at 1600 r min^{-1}. (c) LSV curves of the FeO_x-N/C at various rotating rates, inset is the K-L lines. (d) RRDE LSV curves of the FeO_x-N/C in O_2 saturated electrolytes at 1600 r min^{-1}. (e) n and H_2O_2 with respect to voltage. (f) i-t curves at 0.73 V for the Pt/C and FeO_x-N/C

$$n = \frac{4|I_d|}{|I_d| + |I_r/N|} \quad (2)$$

where i_d and i_r are the disk and ring current, respectively. N is 0.39 and represents the Pt ring current collection efficiency. As shown in Fig. 5e, n is 3.9–3.95 in the range of 0–0.9 V, further indicating that the ORR is a 4e$^-$ reaction. The $E_{1/2}$ for the LSV from the RRDE is 0.84 V, slightly lower than that from the RDE. Similar results can be obtained in several other works[45,46]. The yield of H_2O_2 in 0–0.9 V is less than 10%, agreeing well with the results from the RDE. The electrochemical stability result (Fig. 5f) exhibits that the FeO_x-N/C and Pt/C catalysts maintain about 92% and 83% relative current after the continuous test of 34 000 s, indicating the better catalytic stability of the FeO_x-N/C than that of Pt/C.

Acidic proton exchange membrane fuel cells (PEMFCs) are the promising kind of fuel cells for the proton conducting Nafion membranes available commercially. Therefore, the catalytic activity in acid electrolyte is of high interested[26]. The catalytic performance of the FeO_x-N/C was also investigated in 0.5 mol L^{-1} H_2SO_4, and the results are presented in Fig. 6. In N_2 and O_2 saturated electrolyte, the CV (Fig. 6a) shows an obvious reduction current increase when the electrolyte is saturated with O_2 at 0.88 V, implying the good catalytic activity of the FeO_x-N/C toward the ORR. The LSVs at all rotational speeds are presented in Fig. 6b, exhibiting an onset potential of 0.88 V, closing to the Pt/C. Based on the K-L lines (Fig. 6c) obtained, the electron transfer number (n) is calculated to be in the range of 3.63–3.94, indicating that the ORR on the FeO_x-N/C is a 4-e process in acidic electrolyte of 0.5 mol L^{-1} H_2SO_4. Consequently, the FeO_x-N/C obtained in the present work has the high ORR activity in both basic and acidic electrolytes.

To investigate the practical application of the FeO_x-N/C catalyst, a Zn-Air battery (ZAB) was assembled and its structure is illustrated in Fig. 7a. The ZAB is determined to hardly work in the absence of catalyst (Fig. 7b). When the FeO_x-N/C is applied, the open circuit voltage of the ZAB is 1.5 V, and its current density and peak power density can reach 400 mA·cm^{-2} and 190 mW·cm^{-2}, respectively. This battery performance is higher than reported ones with other cathode materials, such as the Fe, N-doped 3D porous carbon (112 mW·cm^{-2}) [1], the Pt/C+RuO_2 catalysts (80 mW·cm^{-2})[47] , and the Co, N-graphene (50 mW·cm^{-2})[48]. The ZAB can work stability for a long time, as evidenced by the long-time stability test shown in Fig. 7c, and 90% of the initial voltage is retained after the 2-h stability test. The rate performance was investigated using constant current discharge voltage at different current densities. As displayed in Fig. 7d, at various current densities, the values of the discharge voltage are 1.29, 1.26, 1.23 and 1.19 V. When the current densities were as high as 50 mA cm^{-2} discharge is resumed at the end of the discharge of 20, 10, 5 and 2 mA cm^{-2}, the discharge voltages are basically recovered to their original values, which indicates that the catalyst possesses excellent rate performance.

The excellent practical applicability of the FeO_x-N/C for the ORR in the metal-air battery system is displayed. Although this ZAB with the FeO_x-N/C is lower than that with commercial Pt/C, the low price still makes the FeO_x-N/C a promising candidate.

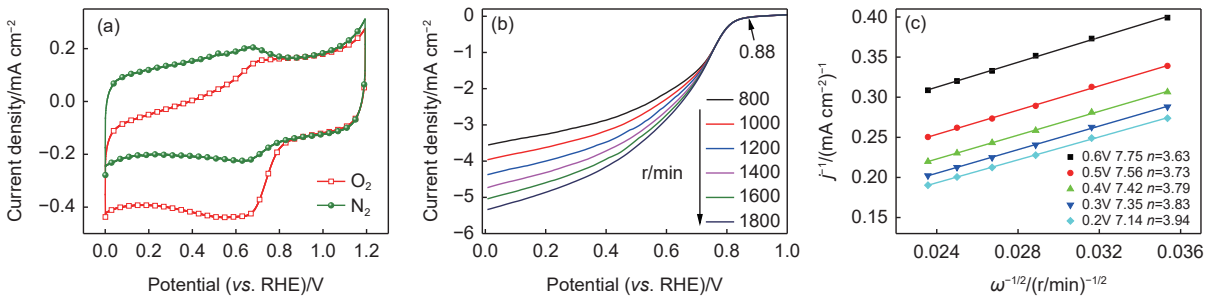

Fig. 6 (a) CV curves of the FeO_x-N/C H_2SO_4 electrolytes (0.5 mol L^{-1}) saturated with O_2 or N_2, (b) LSV curves of the FeO_x-N/C in 0.5 mol L^{-1} H_2SO_4 at various rotating rates, and (c) corresponding K-L lines

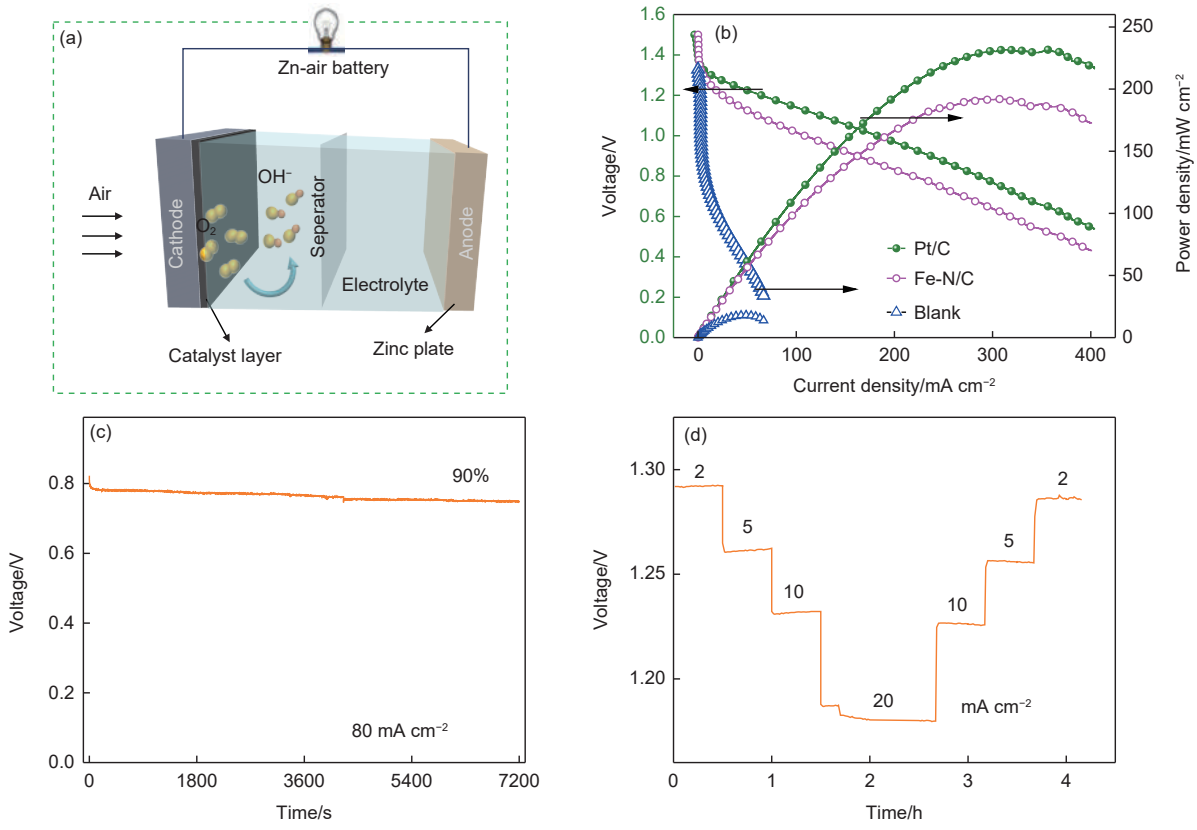

Fig. 7　(a) Diagram of the ZAB with the FeO_x-N/C as cathode catalyst, and (b) its polarization and power density curves, (c) ZAB stability and (d) rate performance

4　Conclusion

Ketjenblack carbon and the PIL of [Hvim]NO_3 are adopted as precursors to successfully synthesize a Fe, N co-doped carbon material (FeO_x-N/C). In the preparation process, the PIL of [Hvim]NO_3 can combine and disperse the additive Fe^{3+} ions, and NO_3^- was thermally pyrolyzed to form the porous structure under the high-temperature calcination. The as-obtained FeO_x-N/C exhibits the unique Fe, N co-doped carbon structure and abundant pores, thus exposing more active sites. In both basic (0.1 mol L^{-1} KOH) and acid (0.5 mol L^{-1} H_2SO_4) electrolytes, the FeO_x-N/C is demonstrated to have the high electrocatalytic activity toward ORR. The onset and $E_{1/2}$ of 1.05 and 0.87 V are obtained in KOH electrolyte, respectively. Subsequently, a zinc-air battery (ZAB) is assembled using the FeO_x-N/C as the cathode catalyst. The ZAB exhibits a peak power density of 185 mW·cm^{-2}. Therefore, the superior ORR activity and simple synthesis method suggest that the FeO_x-N/C catalyst can be probably applied for the fuel cells or metal-air batteries.

Acknowledgements

This work was financially supported by the National Natural Science Foundation of China (21872104, 21776219), China Postdoctoral Science Foundation (2018M631746), the Innovation project of Graduate Students (2022SKY142), and the Basic Research Program of Jiangsu (BK20201213).

References

[1] Huang Y, Liu K, Kan S, et al. Highly dispersed Fe-N_x active sites on graphitic-N dominated porous carbon for synergetic catalysis of oxygen reduction reaction[J]. Carbon, 2021, 171: 1-9.

[2] Zhang Y T, Li S Y, Zhang N N, et al. A carbon catalyst doped with Co and N derived from the metal-organic framework hybrid (ZIF-8@ZIF-67) for efficient oxygen reduction reaction[J]. New Carbon Materials, 2023, 38 (1): 200-209.

[3] Zhang S, Xue H, Li W L, et al. Constructing precise coordination of nickel active sites on hierarchical porous carbon framework for superior oxygen reduction[J]. Small, 2021, 17(35): 2102125-

2102133.

[4] Li J, Zhou Z, Liu K, et al. Co_3O_4/Co-NC modified Ketjenblack carbon as an advanced electrocatalyst for Al-air batteries[J]. Journal of Power Sources, 2017, 343: 30-38.

[5] He X F, Chang L B, Han P F, et al. Highly efficient Co-N-C electrocatalysts with a porous structure for the oxygen reduction reaction[J]. New Carbon Materials, 2023, 38 (5): 976-988.

[6] Wang H Z, Zhao Y Z, Yang Z X, et al. Oxygen-incorporated carbon nitride porous nanosheets for highly efficient photoelectrocatalytic CO_2 reduction to formate[J]. New Carbon Materials, 2022, 37 (6): 1135-1142.

[7] Wang Z L, Xu D, Xu J J, et al. Oxygen electrocatalysts in metal–air batteries: from aqueous to nonaqueous electrolytes[J]. Chemical Society Reviews, 2014, 43 (22): 7746-7786.

[8] Li F, Fu L, Li J, et al. Ag/Fe_3O_4-N-doped ketjenblack carbon composite as highly efficient oxygen reduction catalyst in al-air batteries[J]. Journal of the Electrochemical Society, 2017, 164(14): A3595-A3601.

[9] Li J, Zhou N, Song J, et al. Cu-MOF-Derived Cu/Cu_2O Nanoparticles and CuN_xC_y species to boost oxygen reduction activity of Ketjenblack carbon in Al–air Battery[J]. ACS Sustainable Chemistry & Engineering, 2018, 6(1): 413-421.

[10] Balkourani G, Brouzgou A, Vecchio C L, et al. Selective electro-oxidation of dopamine on Co or Fe supported onto N-doped ketjenblack[J]. Electrochimica Acta, 2022, 409: 139943-1339953.

[11] Gao J, Ma N, Zhai J, et al. Polymerizable ionic liquid as nitrogen-doping precursor for Co-N-C catalyst with enhanced oxygen reduction activity[J]. Industrial & Engineering Chemistry Research, 2015, 54(32): 7984-7989.

[12] Gao J, Ma N, Zheng Y, et al. Cobalt/nitrogen-doped porous carbon nanosheets derived from polymerizable ionic liquids as bifunctional electrocatalyst for oxygen evolution and oxygen reduction reaction[J]. Chemcatchem, 2017, 9(9): 1601-1609.

[13] Yang W, Yue X, Liu X, et al. IL-derived N, S co-doped ordered mesoporous carbon for high-performance oxygen reduction[J]. Nanoscale, 2015, 7(28): 11956-11961.

[14] Qin T, Zhao J, Shi R, et al. Ionic liquid derived active atomic iron sites anchored on hollow carbon nanospheres for bifunctional oxygen electrocatalysis[J]. Chemical Engineering Journal, 2020, 399: 125656-125669.

[15] Cui F, Deng Q, Zhao H, et al. Ionic liquid promoted synthesis of nitrogen, phosphorus, and fluorine triple-doped mesoporous carbon as metal-free electrocatalyst for oxygen reduction reaction[J]. Ionics, 2020, 26: 4609-4619.

[16] Gao J, He C, Liu J, et al. Polymerizable ionic liquid as a precursor for N, P co-doped carbon toward the oxygen reduction reaction[J]. Catalysis Science & Technology, 2018, 8(4): 1142-1150.

[17] Song X, Li W, Liu X, et al. Oxygen vacancies enable the visible light photoactivity of chromium-implanted TiO_2 nanowires[J]. Journal of Energy Chemistry, 2021, 55: 154-161.

[18] Li Y, Wang X, Wang H, et al. “Pharaoh’s Snakes” reaction-derived carbon with favorable structure and composition as metal-free oxygen reduction reaction electrocatalyst[J]. Catalysts, 2023, 13(7): 1059-1072.

[19] Liu G, He F, Zhang J, et al. Yolk–shell structured Fe_3O_4@ C@ F-TiO_2 microspheres with surface fluorinated as recyclable visible-light driven photocatalysts[J]. Applied Catalysis B: Environmental, 2014, 150: 515-522.

[20] Zhang P, Zhang L, Yang X, et al. Cotton-derived three-dimensional carbon fiber aerogel with hollow nanocapsules and ultrahigh adsorption efficiency in dynamic sewage treatment system[J]. Bioresource Technology, 2024, 399: 130563-113573.

[21] Zhang Y, Wang P, Yang J, et al. Decorating ZIF-67-derived cobalt–nitrogen doped carbon nanocapsules on 3D carbon frameworks for efficient oxygen reduction and oxygen evolution[J]. Carbon, 2021, 177: 344-356.

[22] Okonkwo C A, Li G, Li Y, et al. Liquid nitrogen-controlled direct pyrolysis/KOH activation mediated micro-mesoporous carbon synthesis from castor shell for enhanced performance of supercapacitor electrode[J]. Biomass Conversion and Biorefinery, 2021: 1-12.

[23] Kim M, Kim H S, Yoo S J, et al. The role of pre-defined microporosity in catalytic site formation for the oxygen reduction reaction in iron-and nitrogen-doped carbon materials[J]. Journal of Materials Chemistry A, 2017, 5(8): 4199-4206.

[24] Ferrero G A, Fuertes A B, Sevilla M, et al. Efficient metal-free N-doped mesoporous carbon catalysts for ORR by a template-free approach[J]. Carbon, 2016, 106: 179-187.

[25] Wang K, Wu W, Tang Z, et al. Hierarchically structured Co$(OH)_2$/CoPt/N-CN air cathodes for rechargeable zinc–air batteries[J]. ACS Applied Materials & Interfaces, 2019, 11(5): 4983-4994.

[26] Zhang H, Hwang S, Wang M, et al. Single atomic iron catalysts for oxygen reduction in acidic media: particle size control and thermal activation[J]. Journal of the American Chemical Society, 2017, 139(40): 14143-14149.

[27] Chen X, Wang N, Shen K, et al. MOF-derived isolated Fe atoms implanted in N-doped 3D hierarchical carbon as an efficient ORR electrocatalyst in both alkaline and acidic media[J]. ACS Applied Materials & Interfaces, 2019, 11(29): 25976-25985.

[28] Zhao Y, Nara H, Jiang D, et al. Open-mouthed hollow carbons: systematic studies as cobalt-and nitrogen-doped carbon electrocatalysts for oxygen reduction reaction[J]. Small, 2023: 2304450-2304458.

[29] Li Z, Xu Y, Ren X, et al. Facile synthesis of NiS_2–MoS_2 heterostructured nanoflowers for enhanced overall water splitting

performance[J]. Journal of materials science, 2020, 55: 13892-13904.

[30] Panomsuwan G, Eiad-ua A, Kaewtrakulchai N, et al. Cattail leaf-derived nitrogen-doped carbons via hydrothermal ammonia treatment for electrocatalytic oxygen reduction in an alkaline electrolyte[J]. International Journal of Hydrogen Energy, 2022, 47(59): 24738-24749.

[31] Zhang P, Yang X, Zhao Z, et al. One-step synthesis of flowerlike C/Fe_2O_3 nanosheet assembly with superior adsorption capacity and visible light photocatalytic performance for dye removal[J]. Carbon, 2017, 116: 59-67.

[32] Al Marzouqi F, Selvaraj R, Kim Y. Rapid photocatalytic degradation of acetaminophen and levofloxacin using g-C_3N_4 nanosheets under solar light irradiation[J]. Materials Research Express, 2020, 6 (12): 125538-125548.

[33] Li Y, Fang L, Jin R, et al. Preparation and enhanced visible light photocatalytic activity of novel g-C_3N_4 nanosheets loaded with Ag_2CO_3 nanoparticles[J]. Nanoscale, 2015, 7(2): 758-764.

[34] Yadav R K, Kumar A, Park N J, et al. A highly efficient covalent organic framework film photocatalyst for selective solar fuel production from CO_2[J]. Journal of Materials Chemistry A, 2016, 4 (24): 9413-9418.

[35] Sarki N, Narani A, Naik G, et al. Biowaste carbon supported manganese nanoparticles as an active catalyst for the selective hydrogenation of bio-based aldehydes[J]. Catalysis Today, 2023, 408: 127-138.

[36] Singh B K, Shaikh A, Dusane R O, et al. Nanoporous gold–Nitrogen–doped carbon nano-onions all-solid-state micro-supercapacitor[J]. Nano-Structures & Nano-Objects, 2019, 17: 239-247.

[37] Ortiz B, Saby C, Champagne G, et al. Electrochemical modification of a carbon electrode using aromatic diazonium salts. 2. Electrochemistry of 4-nitrophenyl modified glassy carbon electrodes in aqueous media[J]. Journal of electroanalytical chemistry, 1998, 455(1-2): 75-81.

[38] Moreno-Castilla C, García-Rosero H, Carrasco-Marín F. Synthesis and characterization of solid polymer and carbon spheres derived from an emulsion polymerization reaction of different phenolic compounds with formaldehyde[J]. Colloids and Surfaces A: Physicochemical and Engineering Aspects, 2017, 520: 488-496.

[39] Zhu J, He C, Li Y, et al. One-step synthesis of boron and nitrogen-dual-self-doped graphene sheets as non-metal catalysts for oxygen reduction reaction[J]. Journal of Materials Chemistry A, 2013, 1(46): 14700-14705.

[40] Fechler N, Fellinger T P, Antonietti M. Template-free one-pot synthesis of porous binary and ternary metal nitride@ N-doped carbon composites from ionic liquids[J]. Chemistry of Materials, 2012, 24(4): 713-719.

[41] Li G, Wang X L, Fu J, et al. Pomegranate-inspired design of highly active and durable bifunctional electrocatalysts for rechargeable metal-air batteries[J]. Angewandte Chemie-International Edition, 2016, 55(16): 4977-4982.

[42] Mao H, Liu X, Wu S, et al. Built-in electric fields and interfacial electron modulation: enhancement of oxygen reduction reaction in alkaline seawater[J]. Advanced Energy Materials, 2023, 13(48): 2302251-2302261.

[43] Xie Y, Chen X, Sun K, et al. Direct oxygen-oxygen cleavage through optimizing interatomic distances in dual single-atom electrocatalysts for efficient oxygen reduction reaction[J]. Angewandte Chemie International Edition, 2023, 62 (17): e202301833.

[44] Subramanian P, Schechter A. Electrochemical oxygen reduction activity of cobalt-nitrogen-carbon composite catalyst prepared by single precursor pyrolysis under autogenic pressure[J]. Journal of the Electrochemical Society, 2016, 163 (5): F428-F436.

[45] Wang Z, Li Q K, Zhang C, et al. Hydrogen peroxide generation with 100% faradaic efficiency on metal-free carbon black[J]. ACS Catalysis, 2021, 11 (4): 2454-2459.

[46] Luque-Centeno J M, Martínez-Huerta M, Sebastián D, et al. Bifunctional N-doped graphene Ti and Co nanocomposites for the oxygen reduction and evolution reactions[J]. Renewable Energy, 2018, 125: 182-192.

[47] Gan R, Song Y, Ma C, et al. In situ growth of N-doped carbon nanotubes in Fe-$N_x/Fe_2O_3/Fe_3O_4$-encapsulated carbon sheets for efficient bifunctional oxygen catalysis[J]. Applied Catalysis B: Environmental, 2023, 327: 122443-122452.

[48] Tang C, Wang B, Wang H F, et al. Defect engineering toward atomic Co-N_x-C in hierarchical graphene for rechargeable flexible solid Zn-air batteries[J]. Advanced Materials, 2017, 29(37): 1703185-1703194.